Cell Reports Medicine, Volume *4*

Supplemental information

Targeting neoadjuvant chemotherapy-induced metabolic reprogramming in pancreatic cancer promotes anti-tumor immunity and chemo-response

Rong Tang, Jin Xu, Wei Wang, Qingcai Meng, Chenghao Shao, Yiyin Zhang, Yubin Lei, Zifeng Zhang, Yuan Liu, Qiong Du, Xiangjie Sun, Di Wu, Chen Liang, Jie Hua, Bo Zhang, Xianjun Yu, Si Shi, and Chinese Study Group for Pancreatic Cancer

Supplemental Information

Targeting Neoadjuvant Chemotherapy-induced Metabolic Reprogramming in Pancreatic Cancer Promotes Anti-Tumor Immunity and Chemo-response.

Authors: Rong Tang,[1,2,#] Jin Xu,[1,2,#] Wei Wang,[3,4,#] Qingcai Meng,[1,2,#] Chenghao Shao,[5] Yiyin Zhang,[6] Yubin Lei,[7] Zifeng Zhang,[1,2] Yuan Liu,[2, 8] Qiong Du,[2, 9] Xiangjie Sun,[2, 10] Di Wu,[3,4] Chen Liang,[1,2] Jie Hua,[1,2] Bo Zhang,[1,2] Xianjun Yu,[1,2,*] Si Shi,[3,4,11,*] Chinese Study Group for Pancreatic Cancer

Affiliations:

[1]Department of Pancreatic Surgery, Fudan University Shanghai Cancer Center, Shanghai, China.

[2]Department of Oncology, Shanghai Medical College, Fudan University, Shanghai, China.

[3]Shanghai Pancreatic Cancer Institute, Shanghai, China.

[4]Pancreatic Cancer Institute, Fudan University, Shanghai, China.

[5]Department of Pancreatic-Biliary Surgery, Second Affiliated Hospital of Naval Medical University, Shanghai, China.

[6]Department of General Surgery, Sir Run Run Shaw Hospital, School of Medicine, Zhejiang University, Hangzhou, Zhejiang Province, China.

[7]Key Laboratory of Growth Regulation and Translational Research of Zhejiang Province, School of Life Sciences, Westlake University, Hangzhou, Zhejiang Province, China.

[8]Department of Endoscopy, Fudan University Shanghai Cancer Center, Shanghai, China.

[9]Department of Pharmacy, Fudan University Shanghai Cancer Center, Shangai, China.

[10]Department of Pathology, Fudan University Shanghai Cancer Center, Shangai, China.

[#]These authors contributed equally.

[11]Lead contact

[*]Correspondence: shisi@fudanpci.org (S. S.), yuxianjun@fudan.edu.cn (X. Y.)

Supplementary figures.

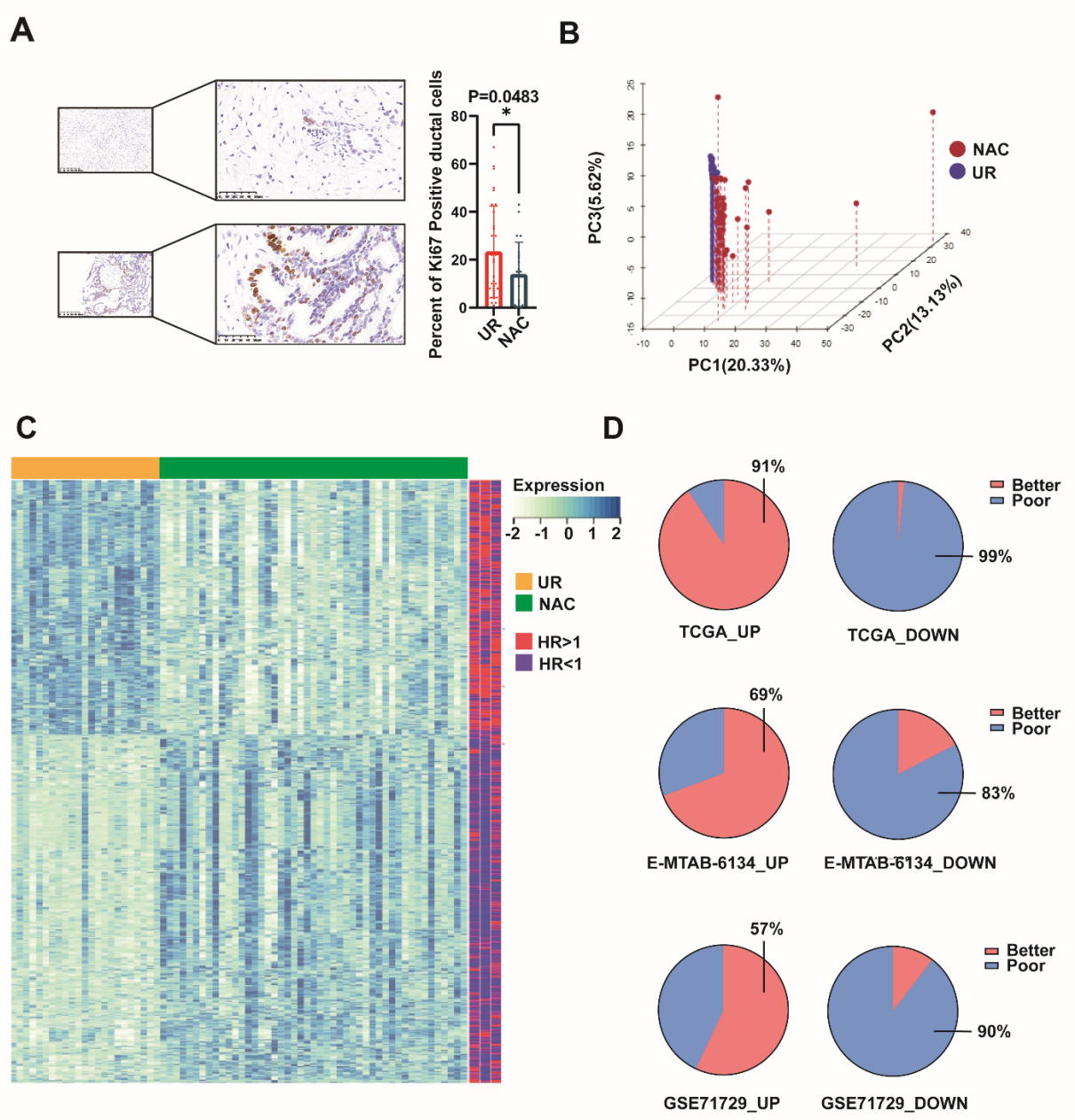

Figure S1. NAC promoted the expression of genes associated with prolonged survival. Related to Figure 1. (A) IHC staining showed the percentage of Ki67+ malignant cells were significantly decreased in PDAC samples that treated with NAC, analyzed by unpaired t test (Mean with standard deviation) (N=54). (B) Three dimensional PCA for NAC and UR PDAC samples based on the differentially expressed genes. (C) Genes upregulated in NAC samples (screened by Wilcoxon test) were associated with prolonged survival interval. (D) The percentage of deregulated genes associated with better or poor prognosis of PDAC.

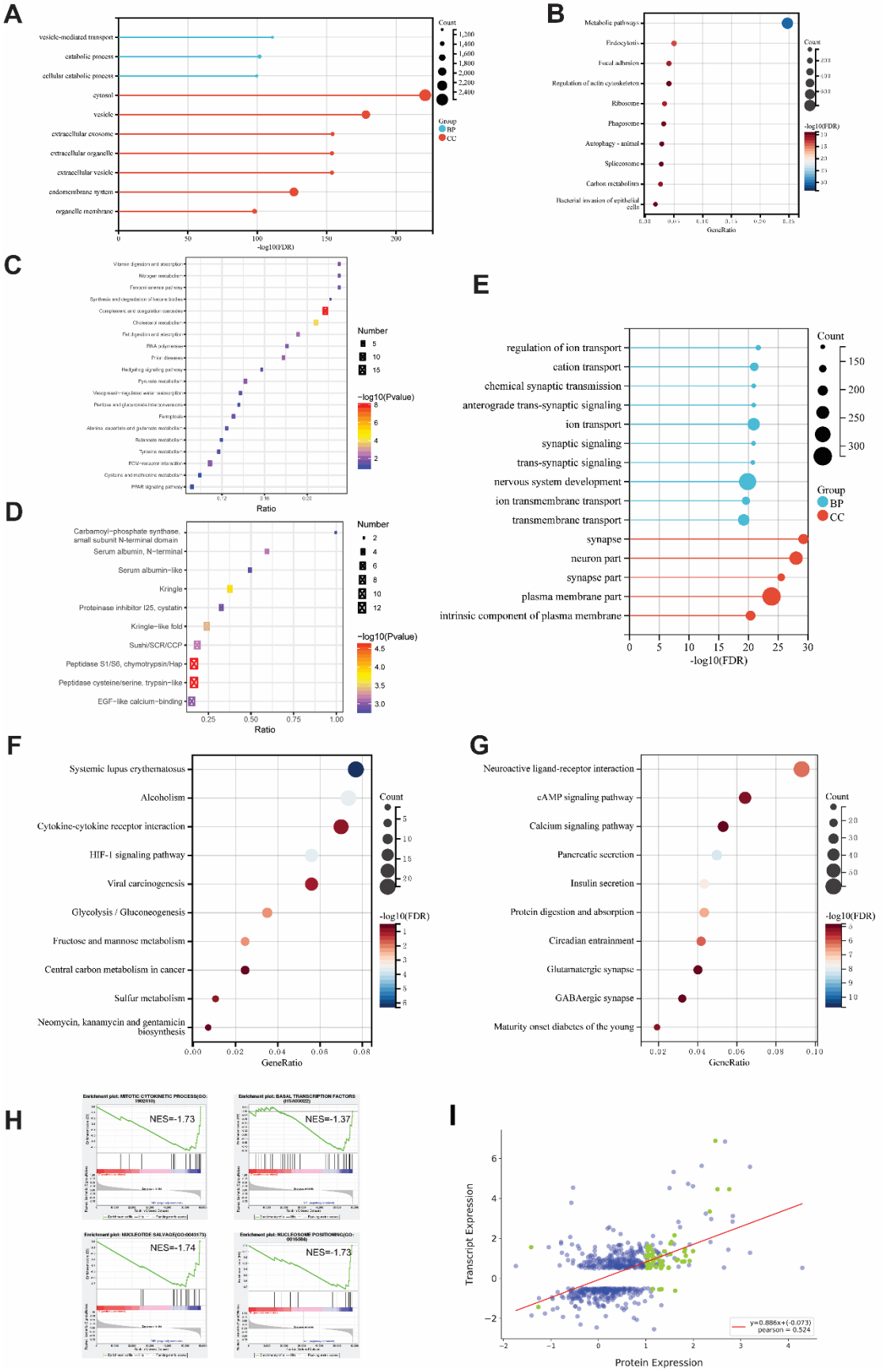
A
vesicle-mediated transport
catabolic process
cellular catabolic process
cytosol
vesicle
extracellular exosome
extracellular organelle
extracellular vesicle
endomembrane system
organelle membrane
Count
Group
BP
CC
-log10(FDR)
B
Metabolic pathways
Endocytosis
Focal adhesion
Regulation of actin cytoskeleton
Ribosome
Phagosome
Autophagy - animal
Spliceosome
Carbon metabolism
Bacterial invasion of epithelial cells
Count
-log10(FDR)
GeneRatio
C
Number
-log10(Pvalue)
Ratio
D
Carbamoyl−phosphate synthase, small subunit N-terminal domain
Serum albumin, N−terminal
Serum albumin−like
Kringle
Proteinase inhibitor I25, cystatin
Kringle−like fold
Sushi/SCR/CCP
Peptidase S1/S6, chymotrypsin/Hap
Peptidase cysteine/serine, trypsin−like
EGF−like calcium−binding
Number
-log10(Pvalue)
Ratio
E
regulation of ion transport
cation transport
chemical synaptic transmission
anterograde trans-synaptic signaling
ion transport
synaptic signaling
trans-synaptic signaling
nervous system development
ion transmembrane transport
transmembrane transport
synapse
neuron part
synapse part
plasma membrane part
intrinsic component of plasma membrane
Count
Group
BP
CC
-log10(FDR)
F
Systemic lupus erythematosus
Alcoholism
Cytokine-cytokine receptor interaction
HIF-1 signaling pathway
Viral carcinogenesis
Glycolysis / Gluconeogenesis
Fructose and mannose metabolism
Central carbon metabolism in cancer
Sulfur metabolism
Neomycin, kanamycin and gentamicin biosynthesis
Count
-log10(FDR)
GeneRatio
G
Neuroactive ligand-receptor interaction
cAMP signaling pathway
Calcium signaling pathway
Pancreatic secretion
Insulin secretion
Protein digestion and absorption
Circadian entrainment
Glutamatergic synapse
GABAergic synapse
Maturity onset diabetes of the young
Count
-log10(FDR)
GeneRatio
H
NES=-1.73
NES=-1.37
NES=-1.74
NES=-1.73
I
Transcript Expression
Protein Expression
y=0.886x+(-0.073)
pearson = 0.524

Figure S2. Functional annotations and enrichment analysis for genes differentially expressed between NAC and UR samples. Related to Figure 1 and Table S4-9.

(A-B) Functional enrichment analyses for all detected proteins in PDAC samples, GO and KEGG annotation, respectively. (C) KEGG analysis for proteins upregulated in NAC group (D) IPR enrichment predicted the function of proteins upregulated in NAC group based on the domain structure. (E) GO enrichment for genes upregulated in NAC group. (F) KEGG enrichment for genes downregulated in NAC group. (G) KEGG enrichment for genes upregulated in NAC group. (H) GSEA for the activity alteration of mitotic cytokinetic process, basal transcription factor, nucleotide salvage and nucleosome positioning between NAC and UR groups. (I) Pearson correlational analysis showed the expression pattern between transcriptome and proteome in PDACs showed high consistency.

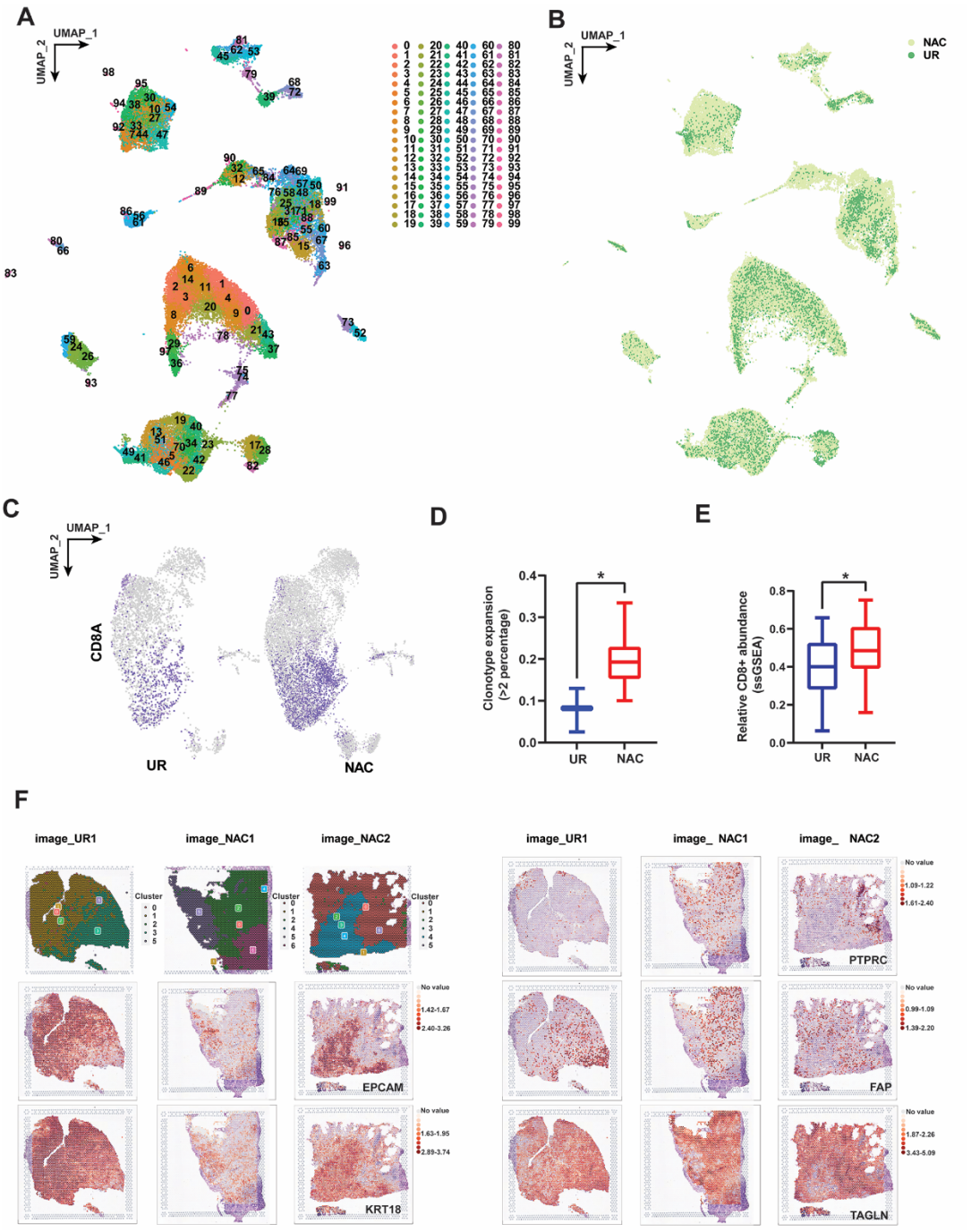

Figure S3. Single-cell and spatial clustering for PDACs with and without NAC. Related to Figure 2 and Figure 3.

(A) UMAP plot showed sequenced cells could be divided into 100 subclusters based on initial clustering. (B) UMAP analysis showed the distribution of cells from samples with and without NAC. (C) The mRNA expression of CD8A in T cells between NAC and UR groups. (D) T cells are featured more clonotype expansion in samples with NAC (Mean with standard deviation). (E) ssGSEA algorithm showed increased CD8+T cell infiltration in samples with NAC based on t test (Mean with standard deviation). (F) Spatially resolved mapping of cell identity markers for

sequenced cells.

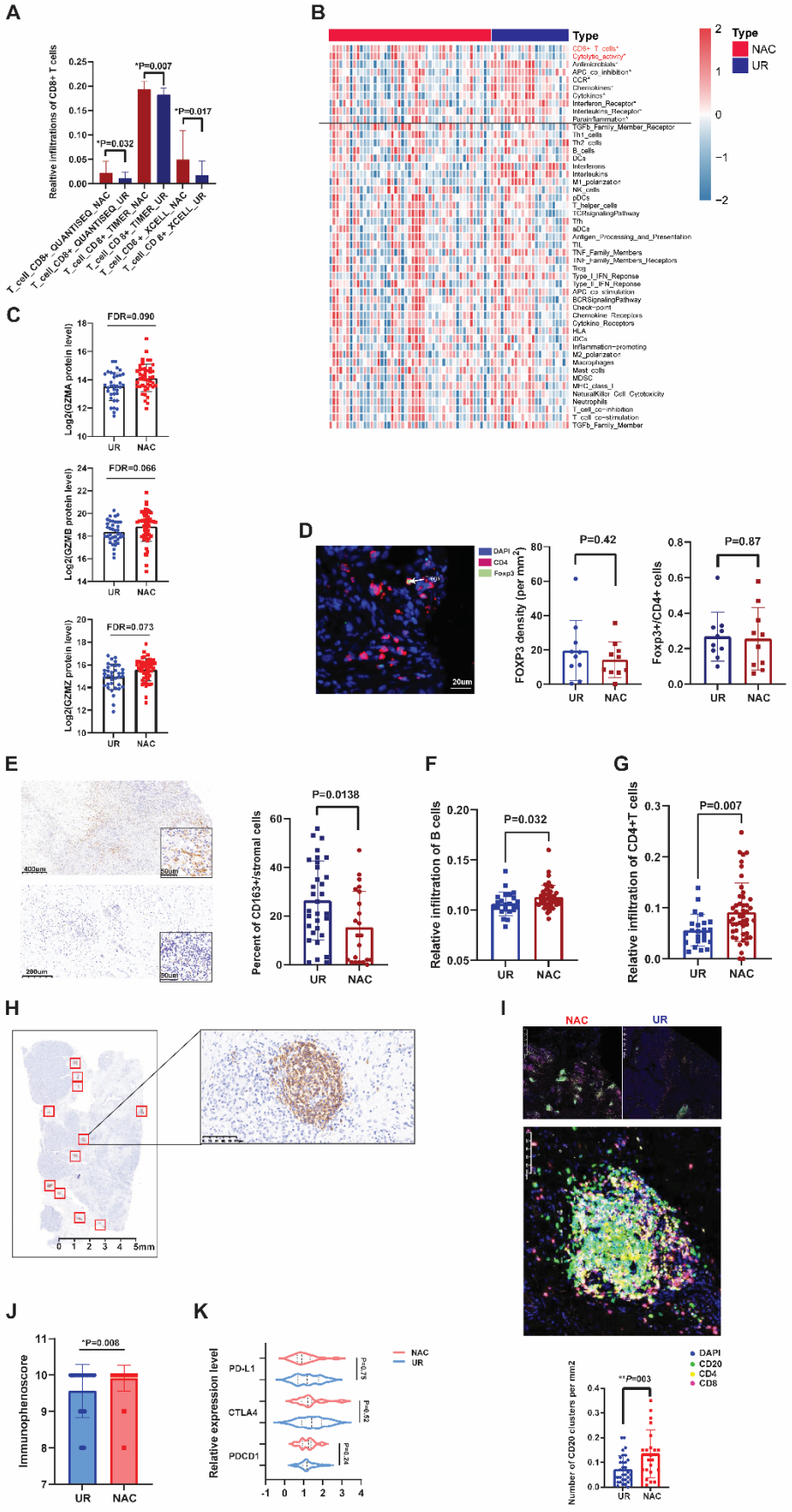
A
Realtive infiltrations of CD8+ T cells
*P=0.032
*P=0.007
*P=0.017
T_cell_CD8+_QUANTISEQ_NAC
T_cell_CD8+_QUANTISEQ_UR
T_cell_CD8+_TIMER_NAC
T_cell_CD8+_TIMER_UR
T_cell_CD8+_XCELL_NAC
T_cell_CD8+_XCELL_UR
B
Type
NAC
UR
C
FDR=0.090
Log2(GZMA protein level)
FDR=0.066
Log2(GZMB protein level)
FDR=0.073
Log2(GZMZ protein level)
UR
NAC
D
DAPI
CD4
Foxp3
20um
P=0.42
FOXP3 density (per mm^2)
P=0.87
Foxp3+/CD4+ cells
E
400um
50um
200um
P=0.0138
Percent of CD163+/stromal cells
F
P=0.032
Relative infiltration of B cells
G
P=0.007
Relative infiltration of CD4+T cells
H
0 1 2 3 4 5mm
I
NAC
UR
DAPI
CD20
CD4
CD8
**P=003
Number of CD20 clusters per mm2
J
*P=0.008
Immunophenoscore
K
Relative expression level
PD-L1
CTLA4
PDCD1
P=0.75
P=6.52
P=0.24

Figure S4. NAC reshaped PDAC immune microenvironment. Related to Figure 2 and Figure 3.

(A) Three independent algorithms supported more CD8+ T cells infiltrated in PDACs which underwent NAC. (B) Heatmap showed differentially activated immune signatures between NAC and UR PDAC samples. (C) Scatter plot showed upregulation trend for protein level of granzymes in PDACs which underwent NAC with marginal significance. (D) The infiltration of Treg cells had no differences between samples treated with NAC and UR. Left panel: representative mIF graph showed the positive staining of Treg cell (N=20). (E) IHC staining showed CD163+ cells infiltrated less in PDACs treated with NAC (N=54). (F-G) B cells and CD4 cells had an increased infiltration in NAC samples, which were based on TIMER and EPIC algorithm, respectively. (H) Demo picture of TLS selection using IHC staining. (I) The density of TLSs was higher in PDACs treated with NAC (N=54). (J) PDAC samples which underwent NAC had an increased immunophenoscore. (K) The expression level of common immune checkpoints had no significant differences between samples treated with NAC and UR. The statistical significance shown in this figure was detected using the t test. Error bars manifested Mean with standard deviation.

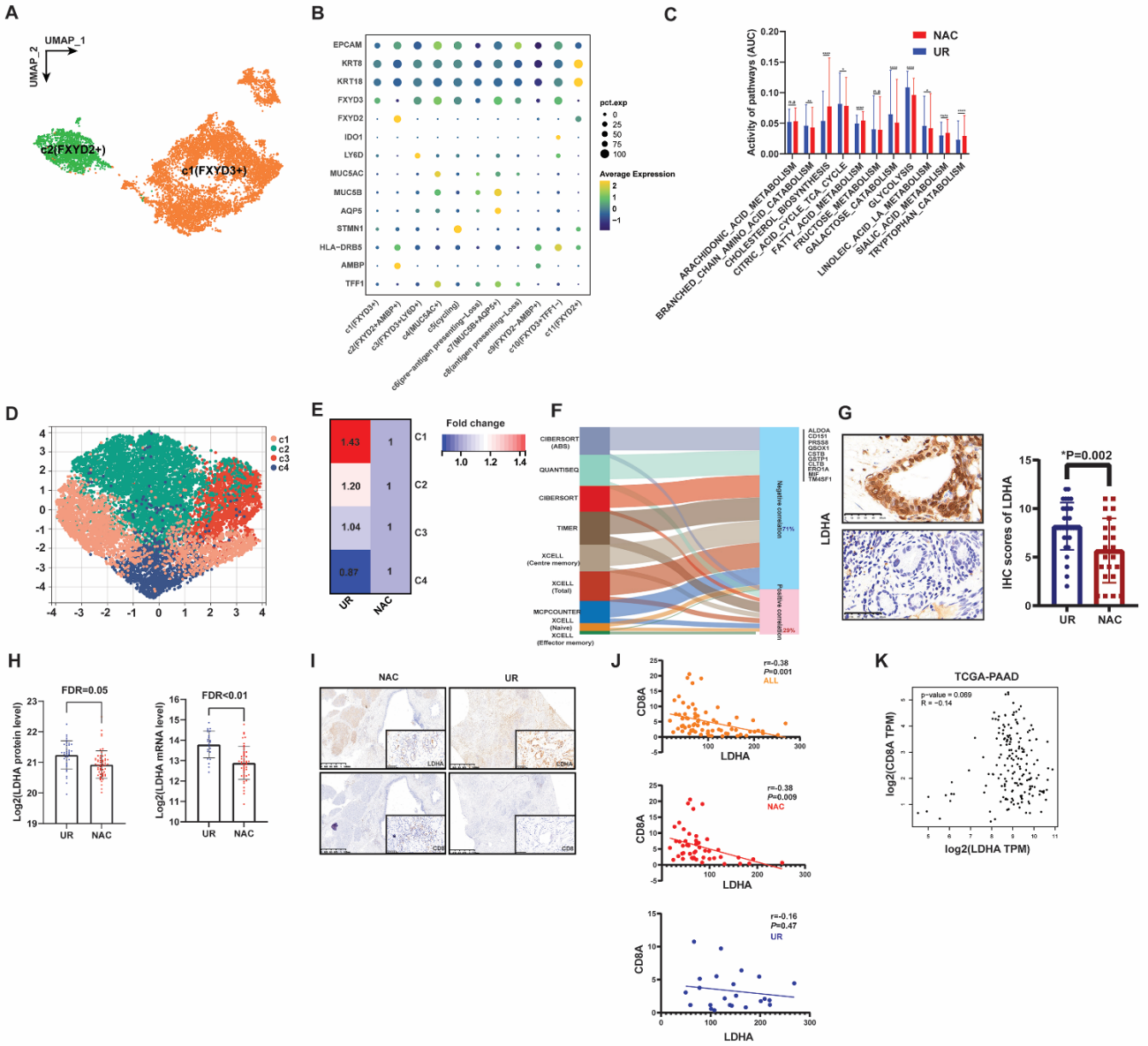

Figure S5. The metabolic reprogramming of PDAC cells is associated with the alteration of immune parameters. Related to Figure 4.

(A) UMAP analysis showed ductal cells could be divided into two major clusters based on the expression of FXYD2 and FXYD3. (B) The presentation of markers for different subclusters of ductal cells. (C) The activity differences of metabolic pathways between ductal cells from samples treated with and without NAC (Mean with Mean with standard deviation). (D) UMAP plot showed that PDAC cells could be classified into four subclusters based on their metabolic activity. (E) Fold change of intensity for C1 to C4 signatures between the MA of NAC and UR samples. (F) The correlation between deregulated metabolism-associated genes and CD8+ T cells' infiltration, which was estimated by multiple algorithms. The deregulated metabolism-associated genes were identified by analyzing the differentially expressed genes between pancreatic ductal cells from PDAC samples with and without NAC. (G) IHC staining showed decreased expression of LDHA in samples received NAC (N=54). Left panel: Representative graph

for positive staining of LDHA in PDAC. (H) Proteome and transcriptome data validated the downregulation trend of LDHA in NAC samples. (I) IHC staining showed an inversed trend in terms of the pattern of LDHA expression and CD8+ T cell infiltration in PDAC samples with and without NAC. (J) The mRNA expression level of LDHA and CD8A were negatively correlated in NAC samples, instead of UR PDACs (K). The correlation between LDHA and CD8A was insignificant in UR PDACs of TCGA dataset. The statistical significance shown in this figure was detected using the t test. Correlational analyses were performed by Pearson approach.

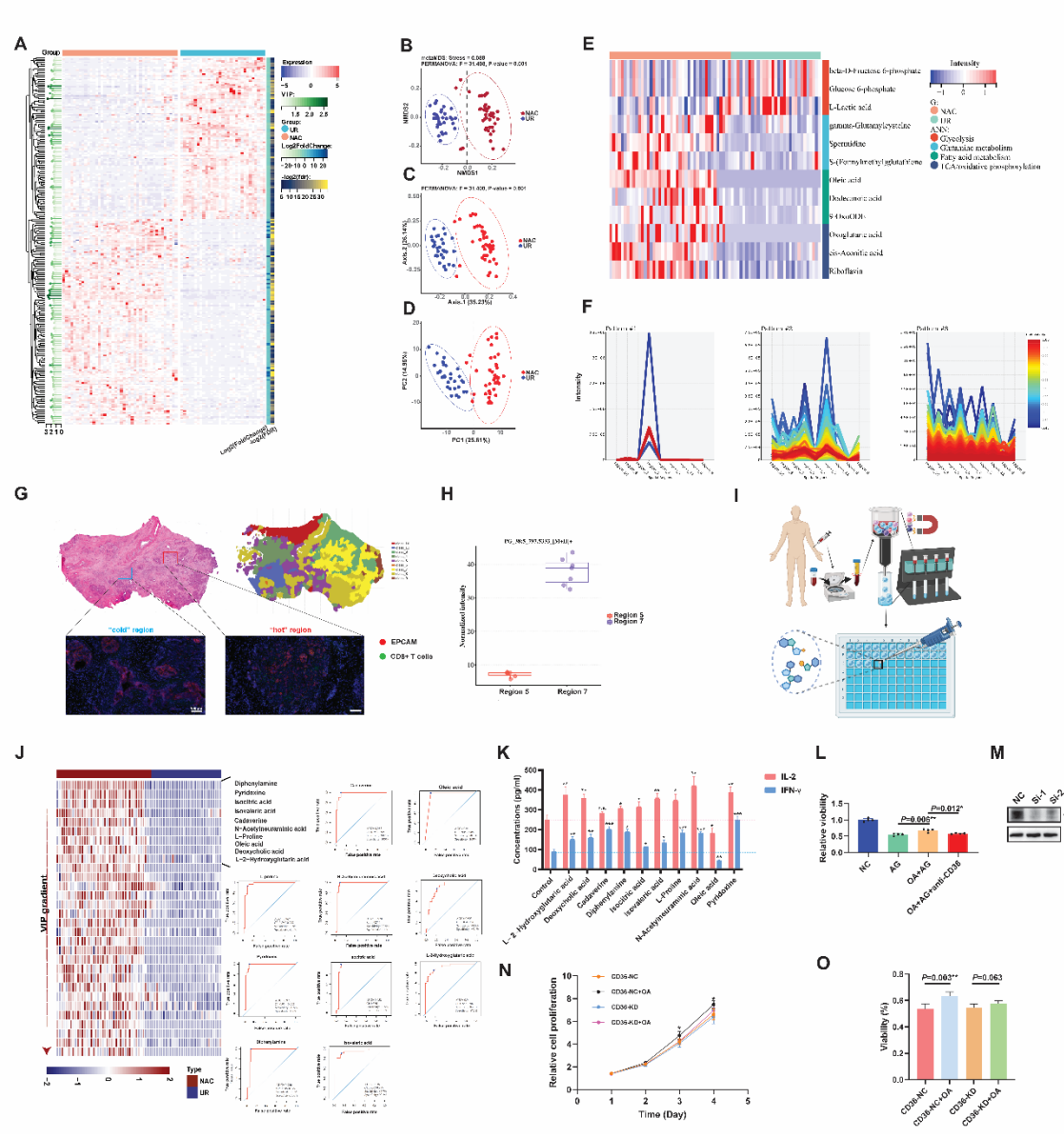

Figure S6. NAC induced metabolome alteration between PDACs with and without NAC. Related to Figure 4 and Figure 5.

(A) Heatmap showed metabolites' abundance was distinct between PDACs with and without NAC. VIP is a statistical measure used to assess the importance of metabolites in multivariate analysis. (B-D) Bray–Curtis NMDS, PCoA and PCA algorithms supported that the difference of metabolome could distinguish NAC and UR PDACs. (E)

A heatmap showed the differences of metabolites in the anaerobic glycolysis, glutamine metabolism, fatty acid utilization and oxidative phosphorylation pathways between NAC and UR samples, which were identified using untargeted metabolome. (F) Spatial-resolved metabolome revealed region-specific metabolic patterns in PDAC. (G) Representative graph of mIF staining showed the distribution of CD8+ T cells in different regions with metabolic difference. (H) PG_38:5 was significantly upregulated in cluster_7 regions compared to cluster_5 regions. (I) Ideograph showed the procedures for T cell separation and stimulation of metabolites. (J) Heatmap panel showed the differentially enriched metabolites and their relevance with treatment states. ROC curves panel showed the accuracy for the metabolites to distinguish different treatment states. (K) Most NAC-induced metabolites promoted T cell function except for oleic acid, which impaired the secretion of cytokines of T cells (N=3). (L) Neutralizing CD36 significantly restrained the chemoresistance induced by oleic acid treatment in pancreatic cancer cells. (M) Western blot validation for the knockdown efficiency of CD36 in panc-1 cells. (N) CCK-8 results showed that knockdown of CD36 blocked the effect of oleic acid on panc-1 cell proliferation (N=5). (O) Oleic acid addition increased the viability of panc-1 cell with AG treatment for 24 hours in CD36-intact condition (N=5).

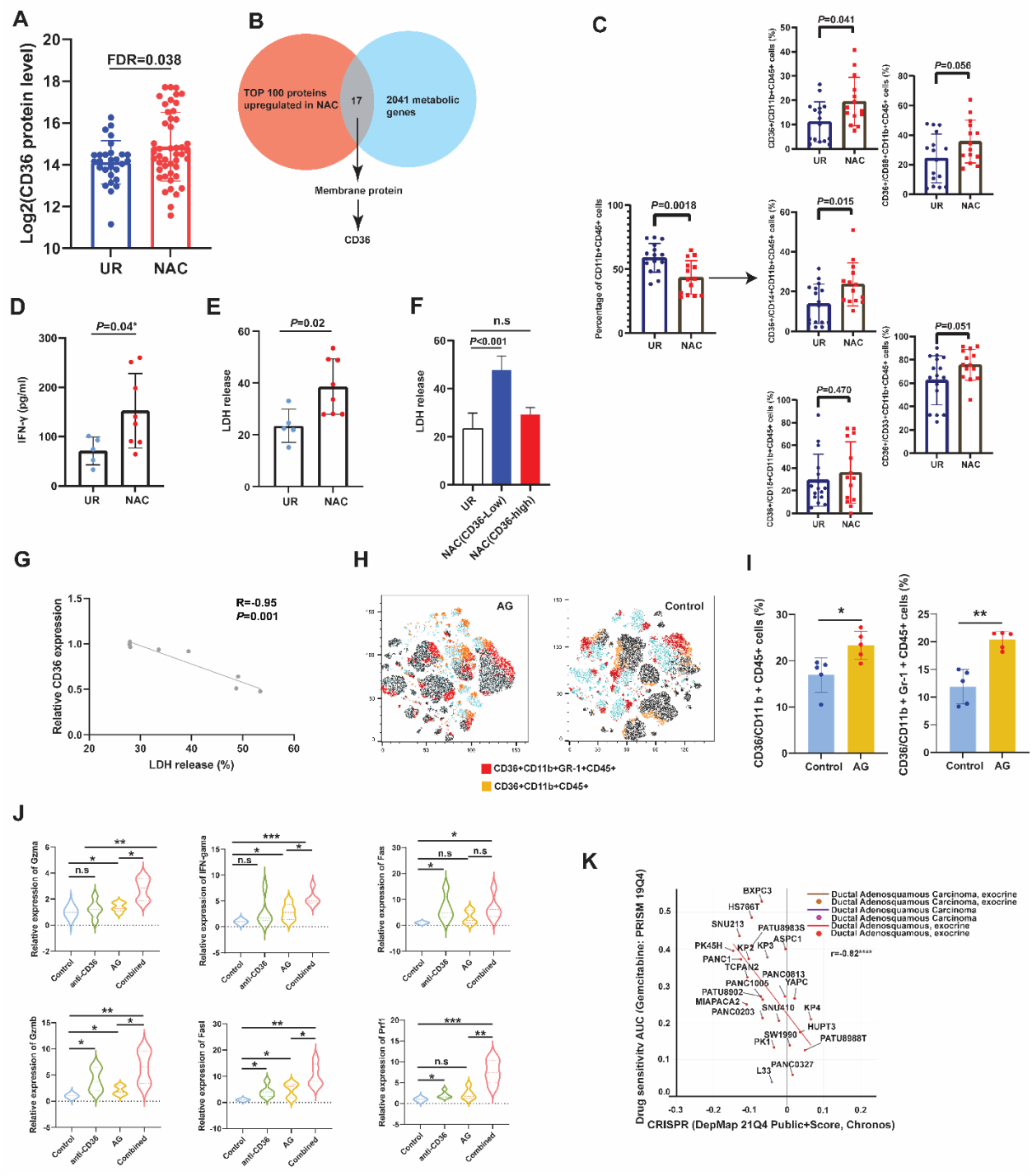

Figure S7. PDAC upregulated CD36 expression after NAC. Related to Figure 6.

(A) Proteome sequencing showed CD36 expression was upregulated in PDAC samples that treated with NAC. (B) Venn plot showed CD36 was the only metabolic membrane protein that upregulated after NAC. (C) Flowcytometry showed CD36 was upregulated in peripheral myeloid-linkage cells. (D) CD8+ T cells treated with lysate from NAC samples showed higher IFN-γ secretion compared to UR samples. (E) CD8+ T cells treated with lysate from NAC samples showed higher cytotoxic performance compared to UR samples, showed by LDH-releasing experiments.

(F) CD8+ T cells treated with lysate from NAC samples with low CD36 expression showed higher cytotoxic performance compared to NAC samples with high CD36 expression, showed by LDH-releasing experiments. (G) CD36 expression in lysate was negatively correlated with LDH releasing level, showed by spearman correlational analysis. (H) TSNE analysis for labeled cell clusters of murine PDAC immune infiltrates by flowcytometry. (I) CD36 had increased distribution on myeloid-linkage cells in harvested murine PDAC after AG treatment. (J) Combination of CD36 blockage and AG synergistically enhanced the expression level of immune-related molecules in murine PDAC (N=5). (K) CD36 expression was more important for pancreatic cancer cells that showed resistance to gemcitabine (based on DepMap database). The statistical significance shown in this figure was detected using t test. Error bars manifested Mean with standard deviation.

Table S1. Characteristics for patients with Proteotranscriptomic sequencing. Related to Figure 1.

Treatment	NAC(N=56)	UR(N=37)
Age at diagnosis (year)		
Mean	58.38	61.22
Range	39-72	43-77
Gender		
Female	30	19
Male	26	18
Tumor location		
Head	19	19
Body-tail	36	17
Multiple site	1	1
Differentiation		
Well	3	0
Well-Moderate	7	5
Moderate	31	22
Moderate-Poor	12	9
Poor	3	1
Lymphovascular invasion		
yes	19	7
no	37	30
Perineural invasion		
yes	49	36
no	7	1

Table S10. Clinical information of samples used for scRNA-seq. Related to Figure 2.

Sample	Gender	Age	Location	Perineural invasion	Vascular invasion	Neoadjuvant
NAC2	Female	66	Neck	+	+	Yes
UR3	Male	49	Head	+	+	No
NAC7	Female	67	Body-tail	-	-	Yes
NAC5	Male	61	Body-tail	+	+	Yes
NAC1	Male	67	Body-tail	-	+	Yes
UR1	Female	70	Body-tail	-	+	No
NAC6	Female	70	Body-tail	-	+	Yes
NAC4	Male	68	Body-tail	+	+	Yes
UR2	Female	51	Head	+	+	No
NAC3	Male	72	Body-tail	-	+	Yes
NAC8	Female	69	Head	-	+	Yes

Table S13. Summary of clinical information for PDAC samples in tissue microarray. Related to Figure 6.

	CD36-Low	CD36-high
Number of patients	128	150
Age (year)		
<=60	54	61
>60	74	89
Gender		
Male	74	89
Female	54	61
Tumor location		
Head	72	81
Body/tail	56	69
T Stage		
T1-2	115	98
T3	35	30
N stage		
N0-1	112	127
N2	16	23
Number of patients with adjuvant AG	32	27
Vascular tumor thrombus		
Yes	40	57
No	88	93
Perineural invasion		
Yes	113	141
No	15	9